Effect of Shear Wall's Eccentricity on the Seismic Performance of RC Dual Structural System

Abbas Ali Tasnimi[1*] and Sayed Mohammad Motovali Emami[2]

1. Professor, Faculty of Civil and Environmental Engineering, Tarbiat Modares University, Iran, * Corresponding Author; email: tasnimi@modares.ac.ir
2. M.Sc. Graduate, Faculty of Civil and Environmental Engineering, Tarbiat Modares University, Iran

Received: 30/01/2013
Accepted: 17/11/2013

ABSTRACT

Reinforced concrete (RC) structural walls are effective for resisting lateral loads induced by earthquakes on building structures. They provide substantial strength and stiffness as well as deformation capacity needed to meet the demands of strong ground motions. In some cases, because of architectural limitations and/or formwork difficulties, the web of shear walls is constructed with an eccentricity with respect to the frame axis. The provision of shear wall's eccentricity may be needed for strengthening of existing building as well. However, most of the reinforced concrete code of practices such as ACI-318-05 and Iranian concrete code (ABA) have no recommendation(s) and/or limitations concerning this eccentricity. In this paper, the effect of Shear Wall's eccentricity on the seismic performance of RC dual system is studied. For this purpose, three two-dimensional (2D) frames with 6, 9 and 12 stories were selected from three-dimensional (3D) buildings, which were analysed and designed according to the third edition of Iranian standard 2800 and ACI-318-02 concrete code of practice. The nonlinear time history and nonlinear static analyses carried out for three different amounts of eccentricities. ABAQUS finite element program is utilized for nonlinear static and time history analysis. To calibrate numerical modelling, experimental results were compared with numerical model results which show good agreement, making sure that the computer numerical simulation of this study is satisfactory. The results indicate that by increasing the eccentricity, the torsional moment of boundary elements and the on-plane bending moment of shear wall significantly increase. In addition, shear wall's eccentricity causes on-plane shear in shear wall.

Keywords:
RC shear wall; Nonlinear static analysis; Nonlinear time history analysis; Eccentricity; Seismic performance

1. Introduction

Reinforced concrete shear walls are effective structural elements for resisting lateral loads imposed by earthquake on building structures. They provide substantial strength and stiffness as well as the deformation capacity needed to meet the demands of strong ground motions. Construction of shear wall causes an increase in strength of building. It is shown that this kind of structure is more economical in comparison with moment resistant frame [1-2]. RC dual system (shear wall+ moment resistant frame) is a ductile and resistant structural system and its response is ductile and flexural [3]. Many cases exhibit that the majority of base shear is borne by shear walls. Boundary elements in shear walls increase flexural capacity and decrease lateral buckling. In addition, boundary element increases resistance and ductility of shear wall [4]. In recent years, many laboratory and analytical researches

have been carried out for improving seismic behaviour of RC dual system that leads to completion of the existing provisions and production of new versions of provisions. Also, many researches have been carried out on RC shear wall and its structural element to provide appropriate seismic performance and ductility of RC dual system [5-7].

In some cases, because of architectural limitations and/or form-work difficulties, the web of shear walls is constructed with an eccentricity with respect to the frame axis. The provision of shear wall's eccentricity may be needed for strengthening of existing buildings. However, most of the RC code of practices such as ACI-318-05 [8] and Iranian concrete code (ABA) [9] have no recommendations and/or limitations concerning this eccentricity.

Larry Roland Jimenez in his MSc dissertation suggested that the reinforced concrete frames strengthened with an eccentric wall and column jackets performed better strength, stiffness, and energy dissipation capacity than similar frames strengthened with an infill wall. He also reported that the out-of-plane displacement due to the torsion created by the eccentricity of the wall did not appear to affect the response. A few diagonal cracks on the inside face of the column were the only indications of the torsion's presence [10].

Bahari [11] focuses on the effect of spandrel beam's eccentricity with respect to coupled shear wall. He founds that the eccentricity of spandrel beam results in 15% decrease in shear capacity of coupled shear walls. This eccentricity also produces on-plane shear force with an amount of 20% of the shear capacity of the wall. He also founds that the eccentricity of spandrel beam has no effect on drift and ductility of coupled shear wall. The lack of research results and practical evident is the main basis for this research work.

The shear wall eccentricity may have destructive effect on performance of shear wall and frame elements. In this paper, the effect of shear wall's eccentricity on seismic performance of RC dual system is studied. For this purpose, three two-dimensional frames with 6, 9 and 12 stories that have different amount of eccentricity were analysed. The nonlinear time history and nonlinear static analysis carried out for the mentioned frames. ABAQUS [12] finite element program is used to carry out nonlinear analyses.

2. Theoretical Background for Modelling

2.1. Concrete Plastic-Damage Model

Behavior of concrete is assumed to obey the plastic-damage model developed by Lee and Fenves [13]. In this model, tensile and compressive damage variables accounted for the different damage states. When concrete is under the application of reversal loads, it differently behaves in tension and compression and hence its stiffness and strength in non-linear region is reduced due to cracking and crushing. Therefore, in either case, the effect is more pronounced as the plastic strain increases. Brief description of the framework for this plastic-damage model and proposed yield condition are described below. According to the incremental theory of plasticity, the strain tensor ε is decomposed into the elastic part (ε^{el}) and the plastic part (ε^{pl}). The strain rate decomposition is assumed for the rate-independent model as below:

$$\dot{\varepsilon} = \dot{\varepsilon}^{el} + \dot{\varepsilon}^{pl} \quad , \quad \varepsilon^{el} = E^{-1}\sigma \tag{1}$$

where $\dot{\varepsilon}$ is the total strain rate, $\dot{\varepsilon}^{el}$ and $\dot{\varepsilon}^{pl}$ are the elastic and plastic parts of the strain rate respectively. The elastic modulus E is a rank four tensor, and σ is the stress tensor. The stress-strain relations for concrete are governed by scalar damaged elasticity:

$$\sigma = K^{el}(\varepsilon - \varepsilon^{pl}) \qquad \text{and} \qquad K^{el} = (1-k)K_o^{el} \tag{2}$$

where K_o^{el} is the initial or undamaged elastic stiffness of the material and K^{el} is the degraded or damaged elastic stiffness; and k is the scalar stiffness degradation variable, which can take values in the range from zero for undamaged material, to one for fully damaged material.

Damage associated with the failure mechanisms i.e., cracking and crushing, results in a reduction of the elastic stiffness. Within the context of the scalar-damage theory, the stiffness degradation is isotropic and characterized by a single degradation variable k. Following the usual notions of continuum damage mechanics, the effective stress is defined as:

$$\bar{\sigma} = K_o^{el}(\varepsilon - \varepsilon^{pl}) \tag{3}$$

The stress is related to the effective stress through the scalar degradation relation:

$$\sigma = (1-k)\bar{\sigma} \tag{4}$$

The value of $(1-k)$ represents the ratio of

effective load-carrying area (i.e., the overall area minus the damaged area) to the overall section area. In the absence of damage it is zero and indicates that the effective stress $\bar{\sigma}$ is coincides with the stress, σ. When damage occurs; however, the effective stress is more representative than the stress, because it is the effective stress area that is resisting the external loads. It is, therefore, convenient to formulate the plasticity problem in terms of the effective stress.

2.2. Hardening Variables

The equivalent plastic strains in tension ($\tilde{\varepsilon}_t^{pl}$) and equivalent plastic strains in compression ($\tilde{\varepsilon}_c^{pl}$), are referred to as independent variables to specify damage states in tension and compression respectively. It is assumed that the micro cracking and crushing in concrete are represented by increasing values of the hardening variables. These variables control the evolution of the yield surface and the elastic stiffness degradation. They are also referred to the dissipated fracture energy required to generate micro-cracks. Because tensile and compressive damages are quite different in concrete, it is not possible to represent all damage states by a single parameter. To account for the different damage responses of concrete in tension and compression, a multi-hardening (or multi-softening) yield function is used. This function has more than one variable to describe the obtained yield surface. If two state variables σ_t and σ_c represent the uniaxial tensile strength and compressive strength of concrete, respectively, the admissible isotropic yield function is constrained by the following condition:

$$F(\sigma, \sigma_t, \sigma_c) \le 0 \tag{5}$$

In the stress space, the yield function is assumed as a first-degree homogeneous function with respect to all three variables. In the present model, the uniaxial strength function is expressed in terms of two damage parameters k_t and k_c given below:

$$\sigma_t = \sigma_t(k_t) \quad , \quad \sigma_c = \sigma_c(k_c) \tag{6}$$

Assuming that both relations in Eq. (6) can be factored into the degradation damage and the effective-stress responses for both tension and compression state yields.

$$\sigma_t = (1 - k_t)\bar{\sigma}_t \tag{7}$$

$$\sigma_c = (1 - k_c)\bar{\sigma}_c \tag{8}$$

The single degradation damage k can be used to describe both tensile and compressive degradation responses as bellow:

$$k = k(\tilde{\varepsilon}^{pl}) = 1 - (1 - k_t)(1 - k_c) \tag{9}$$

Note that k in Eq. (9) satisfies the constraint $0 \le k < 1$ and it is k_t and k_c for uniaxial tensile and compressive case, respectively. Since F is a first-degree homogeneous function and the definition of k in Eq. (9) does hold, the yield function can be written as:

$$F(\bar{\sigma}, \tilde{\varepsilon}^{pl}) \le 0 \tag{10}$$

2.3. Damage and Stiffness Degradation

The equations of the hardening variable $\tilde{\varepsilon}_t^{pl}$ and $\tilde{\varepsilon}_c^{pl}$ could conveniently be formulated by considering uniaxial loading conditions that can be extended to multi-axial states. It is assumed that the uniaxial stress-strain curves for tension and compression can be converted into stress versus plastic strain curves in the simple form of:

$$\sigma_t = \sigma_t(\tilde{\varepsilon}_t^{pl}, \dot{\tilde{\varepsilon}}_t^{pl}) \tag{11}$$

$$\sigma_c = \sigma_c(\tilde{\varepsilon}_c^{pl}, \dot{\tilde{\varepsilon}}_c^{pl}) \tag{12}$$

The equivalent plastic strains could be evaluated by $\tilde{\varepsilon}_t^{pl} = \int_0^t \dot{\tilde{\varepsilon}}_t^{pl} dt$ and $\tilde{\varepsilon}_c^{pl} = \int_0^t \dot{\tilde{\varepsilon}}_c^{pl} dt$, respectively. When the concrete specimen is unloaded from any point on the strain softening branch of the stress-strain curves, the unloading response is observed to be weakened, that is the elastic stiffness of the material appears to be damaged (degraded). The degradation of the elastic stiffness is significantly different between tension and compression tests. Hence in either case, the effect is more pronounced as the plastic strain increases. The degraded response of concrete is characterized by two independent uniaxial damage variable, k_t and k_c which are assumed to be functions of the equivalent plastic strains.

$$k_t = k_t(\tilde{\varepsilon}_t^{pl}), (0 \le k_t \le 1) \tag{13}$$

$$k_c = k_d(\tilde{\varepsilon}_c^{pl}), (0 \le k_c \le 1) \tag{14}$$

The uniaxial degradation variables are increasing functions of the equivalent plastic strains. They can take values ranging from zero to one, for undamaged and fully damaged material, respectively. If E_o is the initial (undamaged) elastic modulus of material, the

stress-strain relations under uniaxial tension and compression loading are respectively:

$$\sigma_t = (1-k_t)E_o(\varepsilon_t - \tilde{\varepsilon}_t^{pl}) \tag{15}$$

$$\sigma_c = (1-k_c)E_o(\varepsilon_c - \tilde{\varepsilon}_c^{pl}) \tag{16}$$

Under uniaxial loading, cracks propagate in a direction transverse to the stress direction. The distribution and propagation of crack, therefore, causes a reduction of the available load-carrying area, which in turn leads to an increase in the effective stress. The effect is less pronounced under compressive loading since cracks run parallel to the loading direction. However, after a significant amount of crushing, the effective load-carrying area is also significantly reduced. The effective uniaxial stresses are given as:

$$\bar{\sigma}_t = \frac{\sigma_t}{(1-k_t)} = E_o(\varepsilon_t - \tilde{\varepsilon}_t^{pl}) \tag{17}$$

$$\bar{\sigma}_c = \frac{\sigma_c}{(1-k_c)} = E_o(\varepsilon_c - \tilde{\varepsilon}_c^{pl}) \tag{18}$$

The effective uniaxial stresses determine the size of the yield (or failure) surface.

2.4. Yield Condition

The plastic damage model uses a yield condition in the following form:

$$F(\bar{\sigma}, \tilde{\varepsilon}^{pl}) = \frac{1}{1-\alpha}\left(\bar{q} - 3\alpha\,\bar{p} + \beta(\tilde{\varepsilon}^{pl})\left\langle \hat{\bar{\sigma}}_{\max}\right\rangle - \gamma\left\langle -\hat{\bar{\sigma}}_{\max}\right\rangle\right) - \bar{\sigma}_c(\tilde{\varepsilon}^{pl}) \le 0 \tag{19}$$

where γ and α are dimensionless material constants, $\bar{p}$ is the effective hydrostatic pressure, $\bar{q}$ is the Von-Mises equivalent effective stress and $\hat{\bar{\sigma}}_{\max}$ (the algebraically maximum eigenvalue of $\bar{\sigma}$) is the maximum principal stress. The function $\beta(\tilde{\varepsilon}^{pl})$ in this equation is given by:

$$\beta(\tilde{\varepsilon}^{pl}) = \frac{\bar{\sigma}_c(\tilde{\varepsilon}_c^{pl})}{\bar{\sigma}_t(\tilde{\varepsilon}_t^{pl})}(1-\alpha) - (1+\alpha) \tag{20}$$

In this, $\bar{\sigma}_t$ and $\bar{\sigma}_c$ are the effective tensile and compressive stresses, respectively. In biaxial compression, with $\hat{\bar{\sigma}}_{\max} = 0$, Eq. (19) reduces to the well-known Drucker-Prager yield condition. The coefficient α can be determined from the initial equi biaxial and uniaxial compressive yield stress and is limited to $0 \le \alpha \le 0.5$.

The coefficient γ would be only considered when $\hat{\bar{\sigma}}_{\max} < 0$ for triaxial compression stress state. This coefficient can be determined by comparing the yield conditions along the tensile and compressive meridians. Typical yield surfaces and deviatoric plane for plane stress state are shown in Figure (1), respectively.

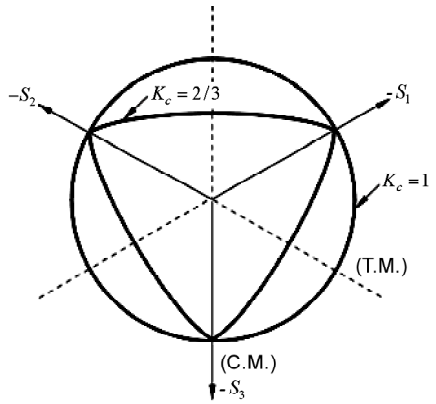

a) Yield Surfaces in the Deviatoric Plane, Corresopoding to Different Value of η_c

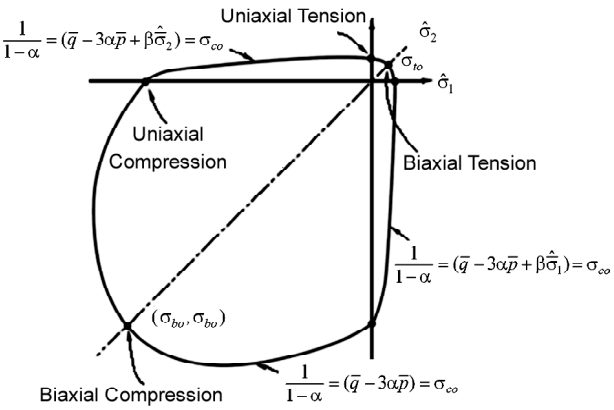

b) Yield Surface in Plane Stress

Figure 1. Yield surfaces in the deviatoric plane and plane stress [12].

2.5. Flow Rule

For this model, the plastic flow which is governed by a flow potential (effective stress space) is based on Drucker-Prager hyperbolic function. Briefly, the elastic-plastic response of the damaged plasticity model is described in terms of the effective stress and the hardening variables.

2.6. Reinforcement Model

Shell element is used to model rebars in the form of surface element in the program. Surface elements

are used to carry rebar layers to represent thin stiffening components in solid elements. This was done by considering the longitudinal and transvers steel bars as separate layers with their specifications such as cross sectional area, spacing and their angle of orientation. The position of rebar layers was specified by their distance from the centroid axes of shear wall.

Embedded element technique was used to model rebar reinforcement (surface element) in solid elements. Embedment considers the perfect bond between concrete and rebars.

2.7. Material Properties

Concrete constitutive behavior is modeled using non-linear constant confinement concrete model proposed by Mander et al. [14], modified by Martinez-Rueda and Elnashai [15] to improve numerical stability under large displacements. The characteristics compressive and tensile strength of concrete used in this research is $f_{ct} = 2.03$ MPa and $f_{ct} = 2.03$ MPa and $f_c = 25$ MPa, $f_c = 25$ MPa respectively. The steel constitutive behavior is modeled using the Menegotto-Pinto steel model [16], which was modified by Filippou et al. [17] and Fragiadakis [18]. The yield and ultimate strength of the rebars that used in this study are 400 Mpa and 600 Mpa, respectively. Figure (2) illustrates the stress-strain curves for material used in this research.

2.8. Nonlinear Analysis by Applying the Explicit Formulae

The general dynamic equation of equilibrium is an ordinary differential equation having constants related to mass (M), damping (C) and stiffness matrices (K) coefficients respectively given in Eq. (21).

$$M\ddot{X} + C\dot{X} + KX = R \tag{21}$$

$X, \dot{X}, \ddot{X}$ and R are the displacement, velocity, acceleration and load vector in time domain, respectively. Central difference method is used to estimate acceleration and velocity with respect to displacement. In this method, it is assumed that:

$$\ddot{X}^t = \frac{1}{\Delta t^2}(X^{t-\Delta t} - 2X^t + X^{t+\Delta t}) \tag{22}$$

Error in (22) is of the order (Δt^2). To have the same order of error in velocity formulae, the following equation can be used:

$$\dot{X}^t = \frac{1}{2\Delta t}(X^{t-\Delta t} + X^{t+\Delta t}) \tag{23}$$

The response for displacement in the time $(t + \Delta t)$ can be obtained using the equation;

$$M\ddot{X}^t + C\dot{X}^t + KX^t = R^t \tag{24}$$

Substituting $M\ddot{X}^t$, $\dot{X}^t$ in Eq. (24), we embark on Eq. (25):

$$\left(\frac{1}{\Delta t^2}M + \frac{1}{2\Delta t}C\right)X^{t+\Delta t} = R^t - \left(K - \frac{2M}{\Delta t^2}\right)X^t - \left(\frac{1}{\Delta t^2}M - \frac{1}{2\Delta t}C\right)X^{t-\Delta t} \tag{25}$$

Using Eq. (25), the term $X^{t-\Delta t}$ can be obtained. This integration is an explicit method in which the displacement is independent of acceleration for time (t), and velocity and displacement for the time $(t + \Delta t)$ can be obtained by using the above equations in time (t). This method is a very simple explicit step-by-step method. However, it is only conditionally stable and will blow up if the time step is not made short enough. It is clear that more

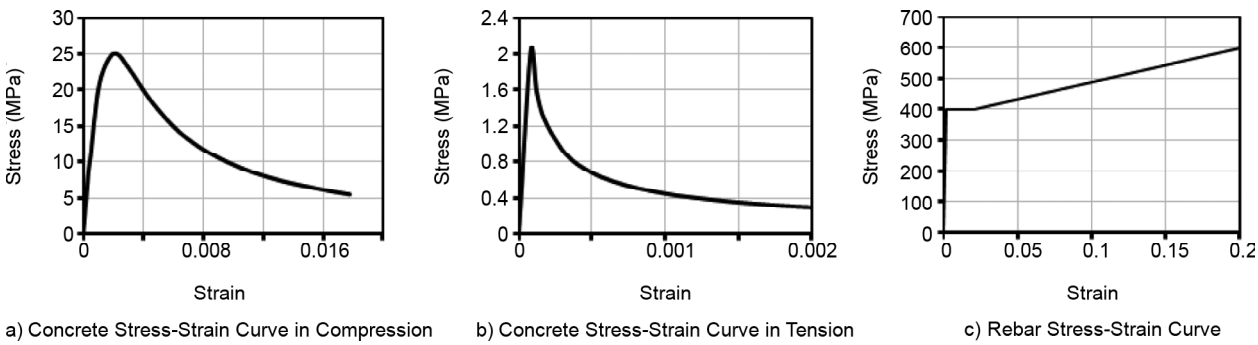

a) Concrete Stress-Strain Curve in Compression b) Concrete Stress-Strain Curve in Tension c) Rebar Stress-Strain Curve

Figure 2. Stress-strain relationship of concrete and steel reinforcement.

effective methods are available, but this method is the simplest procedure and by adopting a shorter time step than others can be used to get a satisfactory representation of the dynamic input and response. In this method, in order to satisfy the convergence of analysis, the time increment of Δt should be less than Δt_{cr} :

$$\Delta t_{cr} = \frac{l_t . l_e}{c} \tag{26}$$

where $l_e =$ 0.7-0.9, $l_t = 0.7$-0.9, l_e is the smallest element dimension, $c = \sqrt{E/\rho}$ and E and ρ are elastic modulus and density of material used, respectively.

2.9. Numerical Verification

In this section, two tested RC shear walls (B2 and RW2) are modelled and analysed in 2D cases using ABAQUS framework. The strength and nonlinear behaviour of the tested walls in the form of capacity curves are compared with the same numerical results. The nonlinear behaviour and failure modes of the shear wall B2 was tested by Oesterle et al. [19] in Portland Cement Association and the study on RW2 performed by Thomsen and Wallace [20] in Clarkson University of New York. The specification of these walls is shown in Figures (3) and (4), and their material properties are presented in Table (1). The plasticity parameters corresponding to concrete damage plasticity (CDP) model used for numerical modelling of both walls are listed In Table (2).These values are the default plasticity parameters of CDP in ABAQUS. Idealized trilinear stress-strain relationship is used for modelling

Table 1. Material properties of specimens B2 and RW2 [19-20].

Specimen	Zone	Concrete		Reinforcement			
				Horizontal		Vertical	
		f'_c (MPa)	E_c (MPa)	ρ (%)	f_y (MPa)	ρ (%)	f_y (MPa)
B2	Web	53.6	32700	0.63	532	0.29	532
	Boundary Element	53.6	32700	0.63	532	3.67	410
				Main Bars		Tie Reinforcement	
		f'_c (MPa)	E_c (MPa)	Φ (mm)	f_y (MPa)	Φ (mm)	f_y (MPa)
RW2	Web	42.8	31030	6.35	414	4.76	448
	Boundary Element	47.6	31030	9.53	414	4.76	448

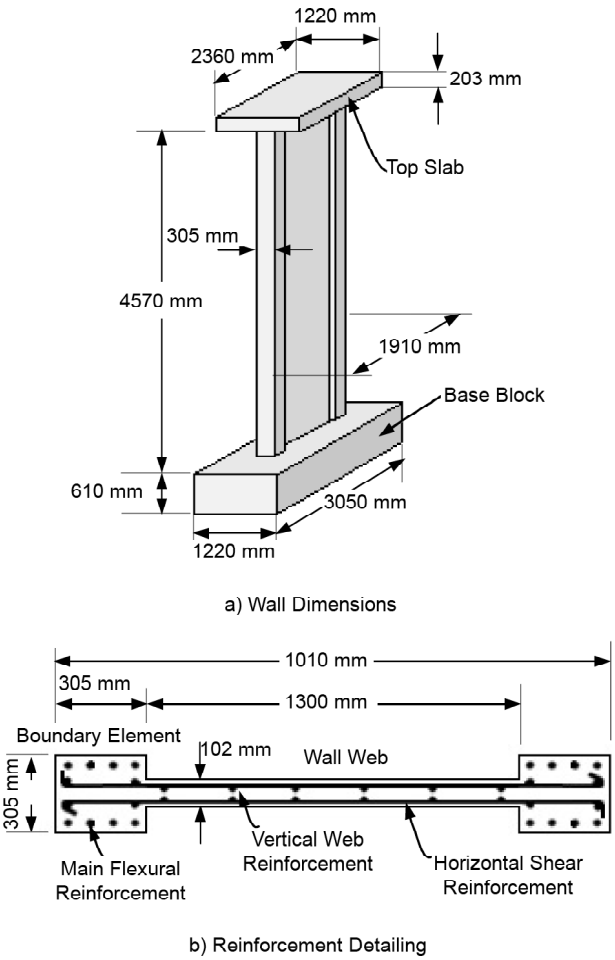

Figure 3. Schematic of test setup and reinforcing of specimen B2 [19].

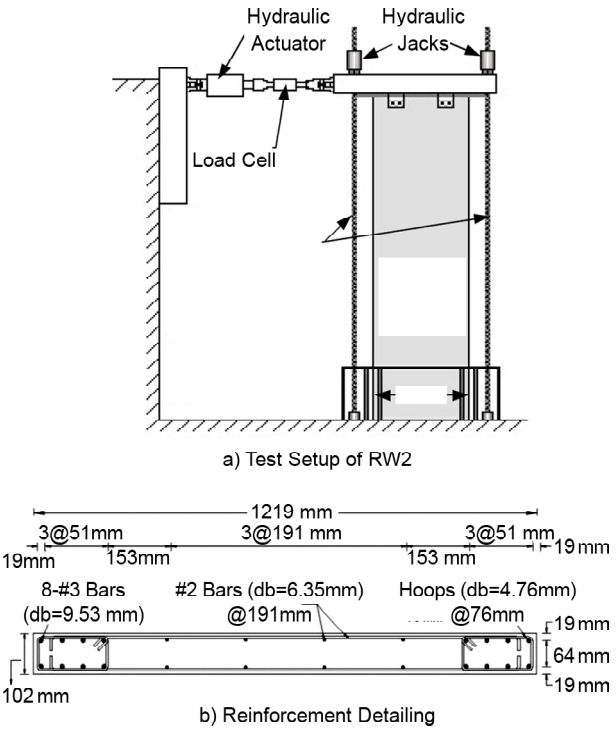

Figure 4. Schematic of test setup and reinforcing of specimen RW2 [20].

Table 2. Plasticity parameters of CDP model for numerical analysis.

Specimen	Dilatation Angle	Eccentricity	f_{bo}/f_{co}	K
B2	30	0.1	1.15	0.667
RW2	30	0.1	1.15	0.667

reinforcement. Figure (5) compares the capacity curve of both B2 and RW2, obtained from analytical results, with the backbone of hysteretic curves from experimental results. It can be seen that the nonlinear behaviour of both walls is predicted with an acceptable degree of precision and have good match in case of stiffness, strength and ductility. Figure (5) shows that the capacity curves in nonlinear range are jagged. In fact, this phenomenon is because of CPD model that use in explicit analysis. Therefore, it can be said that, the results of verification of two experimental walls confirm that outputs of nonlinear analyses in this study are in reliable range.

3. Structures Underinvesttion

Three reinforced concrete frames with various amounts of shear wall eccentricity are selected from three reinforced concrete buildings with 6, 9 and 12 stories having dual structural systems. The buildings were analysed and designed according to the third edition of Iranian standard 2800 for seismic design [21] and ACI318-02 [8] concrete code of practice. The similar plan of building is shown in Figure (6-a). The height of each story is 3m. High seismicity area (0.35 design base acceleration ratio) is considered for the analysis.

The main sample results of the design are listed in Table (3) and the relevant reinforcing details are presented in Figure (6-b, 6-c & 6-d). As it is shown in Figure (6-a), frame of axis-1 (in x direction) is selected from each building. The nonlinear static and nonlinear time history analysis is carried out for the selected structures with different values of eccentricity, using ABAQUS [12] 3D finite element program.

3.1. Modelling of Structures

In this research, nonlinear time history and nonlinear static analyses are performed for 45 RC dual structural systems with 6, 9 and 12 stories. Three eccentricity values were considered to explore the effect of shear wall's eccentricity on seismic performance of RC dual structural systems. Figure (6-e) shows the shear wall with no eccentricity (E0), and Figure (6-f) shows the shear wall with smaller eccentricity (E1). In the case of Figure (6-g) the shear wall's eccentricity is more elaborated in such a manner that the outer face of the frame's columns is attached to the inner face of shear wall with more eccentricity (E2). It should be noted that the amounts of eccentricity in Figure (6) is percentage of eccentricity to boundary element width. For nonlinear static analysis, two types of lateral load distribution suggested by FEMA-356 [22] were applied to push the structures. The first type lateral load distribution is corresponded to the fundamental mode of the structure, and the second type lateral load distribution is uniform consisting of lateral forces proportional to the total mass at each level. Three time history acceleration records from Bam, Tabas and Kojour earthquakes are used for nonlinear time history analyses. Some initials are used as designating codes to

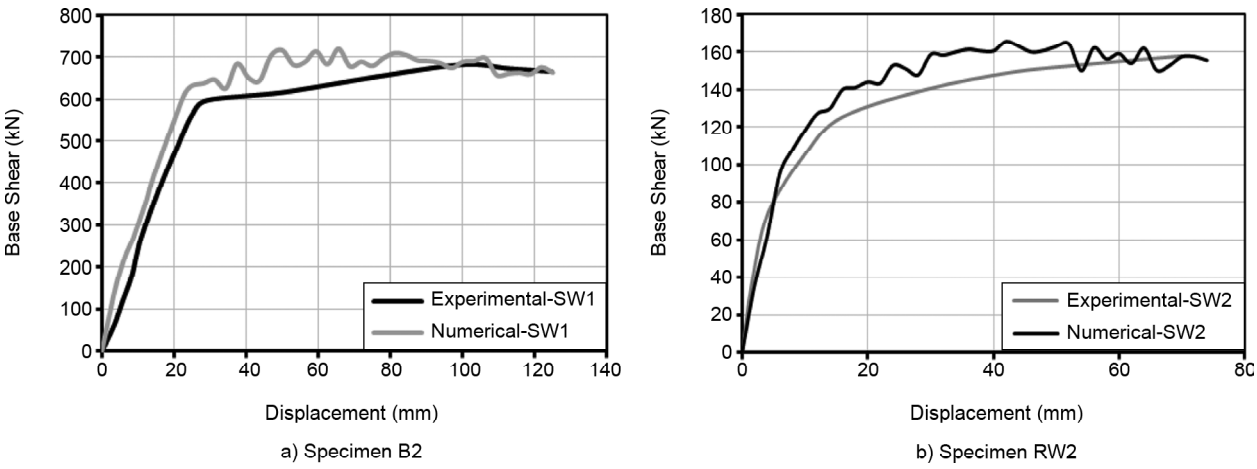

Figure 5. Experimental and analytical capacity curve for walls B2 and RW2.

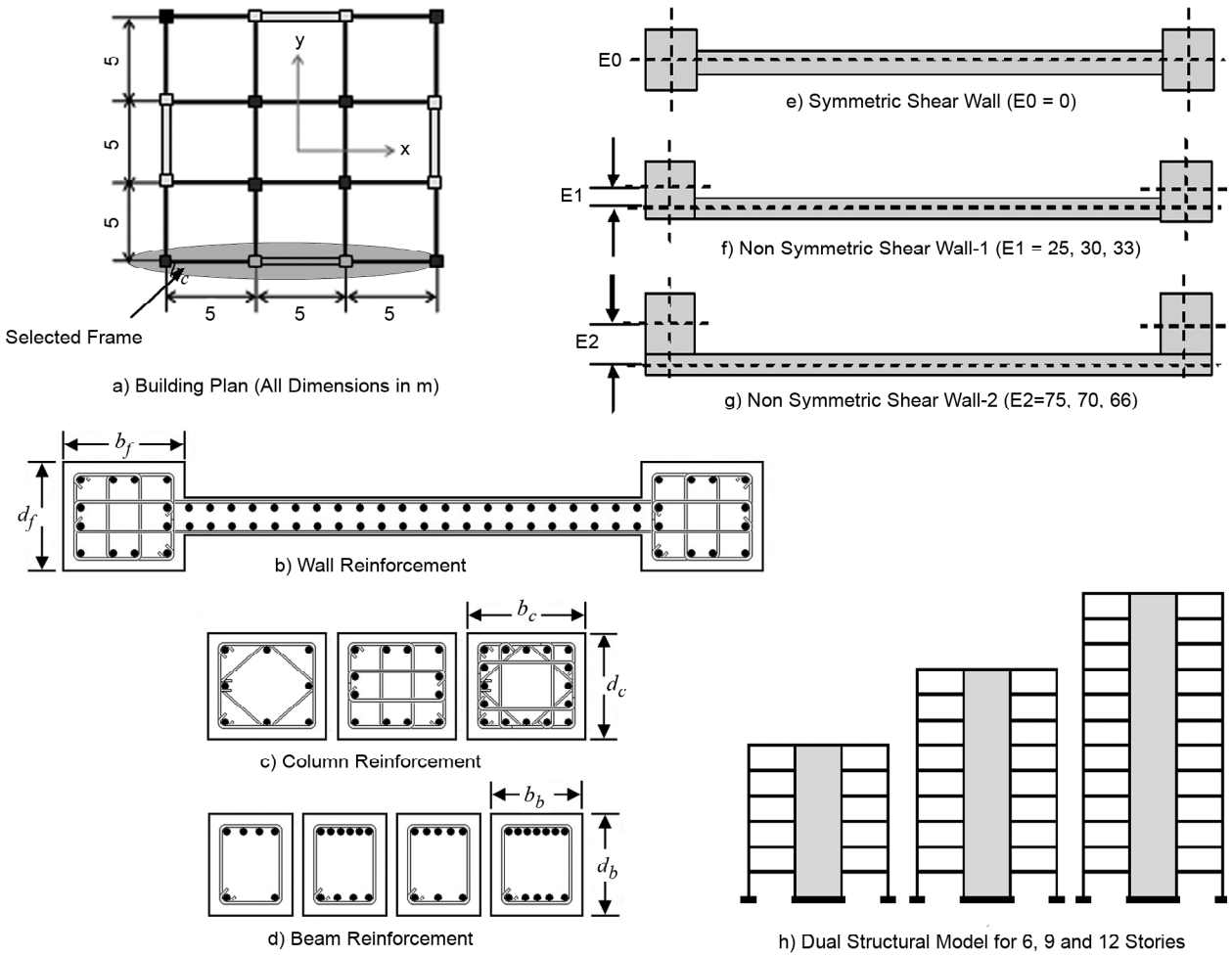

Figure 6. Building plan, dual model and detail of shear wall, column and beam reinforcement.

Table 3. Detail of shear walls, columns and beams section.

Member Specification			Number of Building Story										
			6 Story			9 Story				12 Story			
			4 to 6	2 & 3	1	5 to 9	3 & 4	2	1	8 to 12	5 to 7	3 & 4	2	1
Columns	A_s (mm^2)		4ϕ18	8ϕ18	8ϕ18	8ϕ18	8ϕ18	16ϕ18	16ϕ18	8ϕ18	16ϕ18	16ϕ18	16ϕ18	16ϕ18
	d_c (mm)		300	400	400	300	400	500	500	300	400	500	600	600
	b_c (mm)		300	400	400	300	400	500	500	300	400	500	600	600
Beams	A_s (mm^2)	Top	4ϕ14	4ϕ14	4ϕ14	5ϕ16	5ϕ16	4ϕ16	4ϕ16	6ϕ16	7ϕ16	6ϕ16	6ϕ14	6ϕ14
		Bot	3ϕ14	3ϕ14	3ϕ14	2ϕ16	3ϕ14	3ϕ16	3ϕ16	3ϕ16	4ϕ16	3ϕ16	4ϕ14	4ϕ14
	b_b (mm)		300	400	400	300	400	500	500	300	400	500	600	600
	d_b (mm)		300	300	300	300	300	300	300	300	300	300	300	300
Shear walls	Flanges	A_s (mm^2)	8ϕ18	12ϕ18	16ϕ18	8ϕ18	16ϕ18	20ϕ20	24ϕ20	8ϕ18	16ϕ18	20ϕ24	24ϕ24	24ϕ24
		b_f (mm)	300	400	400	300	400	500	500	300	400	500	600	600
		d_f (mm)	300	400	400	300	400	500	500	300	400	500	600	600
	Webs	A_s (mm^2)	ϕ12@30	ϕ12@200	ϕ12@200	ϕ12@300	ϕ12@150	ϕ12@150	ϕ14@150	ϕ12@300	ϕ12@150	ϕ14@150	ϕ14@150	ϕ16@150
		t_w (mm)	200	200	200	200	200	200	200	200	200	200	200	200
		L_w (mm)	4700	4600	4600	4700	4600	4500	4500	4700	4600	4500	4400	4400

address these structures. Designating codes start with first two or three digits to express the number of stories (6S, 9S or 12S). The next two digits represent the kind of lateral load for the nonlinear static analysis (TL or DL) and to indicate the time history analysis for specified earthquake, "TB" for Bam earthquake, "TT" for Tabas earthquake and "TK" for Kojour earthquake. The last two digits specify the eccentricity value mentioned above. Table (4) gives the designated code for all structures.

Table 4. Designating codes for all 45 dual structural systems.

Non-Linear Static Analysis		Non-Linear Time History Analysis		
1st Type TL	2nd Type DL	Bam Eq.	Tabas Eq.	Kojour Eq.
6STLE0	6SDLE0	6STBE0	6STTE0	6STKE0
6STLE1	6SDLE1	6STBE1	6STTE1	6STKE1
6STLE2	6SDLE2	6STBE2	6STTE2	6STKE2
9STLE0	9SDLE0	9STBE0	9STTE0	9STKE0
9STLE1	9SDLE1	9STBE1	9STTE1	9STKE1
9STLE2	9SDLE2	9STBE2	9STTE2	9STKE2
12STLE0	12SDLE0	12STBE0	12STTE0	12STKE0
12STLE1	12SDLE1	12STBE1	12STTE1	12STKE1
12STLE2	12SDLE2	12STBE2	12STTE2	12STKE2

4. Analysis Result

4.1. Nonlinear Static Analysis

For non-linear static procedure or pushover analysis, 3D finite element computer program ABAQUS [12] was used to predict the building responses. Each building is idealized by a 3-D model. Each floor diaphragm is assumed rigid in its own plane but flexible for out of plane. Because of the rigidity, each floor has three common degrees of freedom comprising two translations and one rotation.

4.1.1. Capacity Curve

Capacity curve for 6, 9 and 12 story structures due to applied lateral loads are shown in Figure (7). The structural models are distinguished by their name in which the first digit refers to the number of stories followed by two characters, "DL" or "TL" indicating the distributed and inverted triangle lateral load respectively, and the last character followed by a digit refer to the amount of eccentricity specified in Figure (6). It should be noted that according to the Iranian standard 2800 [21], the allowable drift for seismic design spectrum is related to the fundamental period (T) of the system and is limited to 2.5% roof drift for $T < 0.7$ s and 2% for $T \geq 0.7$ s. It is evident that the eccentricity of shear wall has no significant effect on the elastic state of behaviour and its effect in nonlinear state of the behaviour is changing with the height of the structure. Figure (7) shows that the capacity of E2 specimen is more than E0 and E1 specimens, but it must be said that this phenomenon has no relevance to the eccentricity of shear walls. In fact, it is because of the more length of shear wall in case of E2 (Figure (6)) that leads to

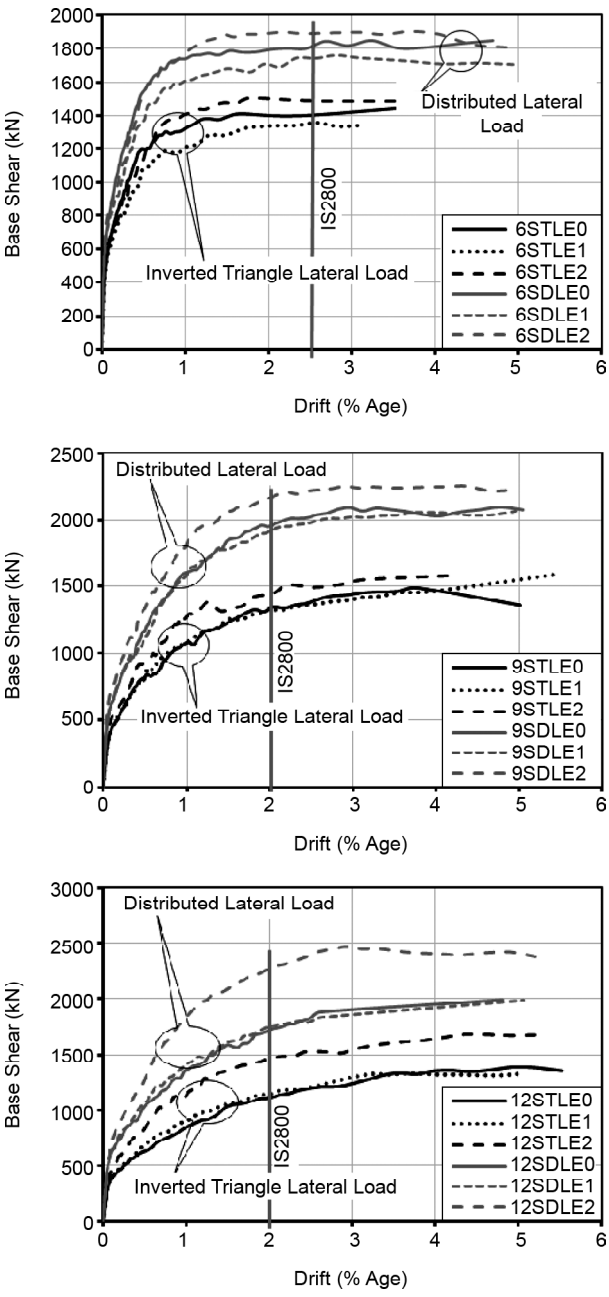

Figure 7. Capacity curve for 6, 9, and 12 story frames under lateral loads.

more capacity in structure. Meanwhile, all structures have more response to the distributed lateral load rather than inverted triangle lateral load and this is more pronounced by increasing the height of the structure, because the moment arm in case of inverted triangular is bigger than that of distributed load. Therefore, the amount of moment that imposes to the base of frame in case of distributed load is less than inverted triangular load (note that the amount of lateral applied load in both cases is the same). One can conclude that strength degradation is more possible in inverted triangle load, because of more imposed moment.

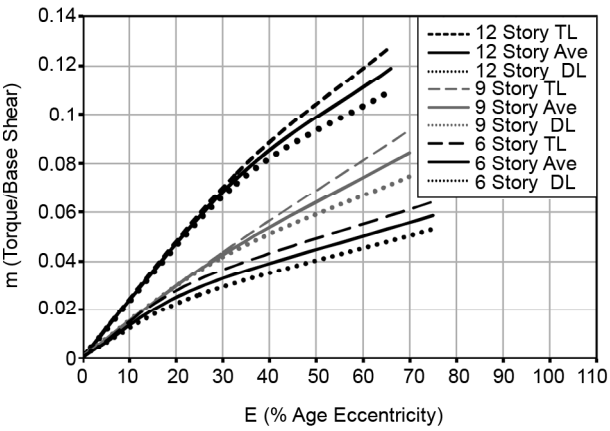

Figure 8. Ratio of boundary element's torsional moment to base shear versus eccentricity.

4.1.2. Torsional Moment

Referring to the results of nonlinear static analysis, eccentricity of shear wall exerts torsional moment on boundary elements. From Figure (7) drift, value accorded with IS2800 is shown and the corresponded base shear is extracted to find their relation with the torsional moment. For each frame, the relationship between torsional moment and base shear is drawn and their linear regression provided the coefficient "*m*" (ratio of torsional moment to base shear). All calculated "*m*" value and the average of each group of frames with the same eccentricity calculated and listed in Table (5). These values indicate that by increasing the amounts of eccentricity and also story height, the ratios of torsional moment to base shear (*m*) increases too. Figure (8) illustrates the ratio of torsional moment to base shear against the eccentricity.

Table 5. "m" and "n" values for Torsional and on-plane moment.

Frame	Eccentricity (%age)	*m* Values	Average "*m*"	*N* Values	Average "*n*"
6TLE0	0	0.0000	0.0000	0.0000	0.0000
6DLE0		0.0000		0.0000	
6TLE1	25	0.0330	0.0295	0.2188	0.1954
6DLE1		0.0260		0.172	
6TLE2	75	0.0640	0.0585	0.4228	0.4064
6DLE2		0.0530		0.3900	
9TLE0	0	0.0000	0.0000	0.000	0.0000
9DLE0		0.0000		0.000	
9TLE1	30	0.0440	0.0430	0.2229	0.2355
9DLE1		0.0420		0.2480	
9TLE2	70	0.0940	0.0845	0.3593	0.3655
9DLE2		0.0750		0.3716	
12TLE0	0	0.0000	0.0000	0.0000	0.0000
12DLE0		0.0000		0.0000	
12TLE1	33	0.0760	0.0740	0.2788	0.2578
12DLE1		0.0720		0.2367	
12TLE2	66	0.1280	0.1190	0.3857	0.3571
12DLE2		0.1100		0.3285	

4.1.3. On-Plane Bending Moment

Other results of nonlinear static analysis are referred to the effect of eccentricity that imposes an on-plane bending moment to the shear wall. In this case, the on-plane bending moment (OPBM) calculated from the numerical analysis are related to base shear of the frames. For each frame, the relationship between base shear and OPBM is drawn and their linear regression provided the coefficient "*n*" (ratio of OPBM to base shear). All calculated "*n*" value and the average for each group of frames with the same eccentricity are listed in columns 5 and 6 of Table (5). These values indicate that by increasing the amount of eccentricity and story height, the "*n*" value slightly increases too. Figure (9a) illustrates the variation of OPBM against base shear for all frames. This indicates that by increasing the base shear, the structure enters to its non-linear behaviour at which state the OPBM decreases. Therefore, the most effect of eccentricity to the OPBM belongs to the linear state of behaviour. In addition, Figure (9b) shows the variation of "*n*" values against the eccentricity and their linear regression provides the coefficient $\alpha = 0.006$. Knowing (α), we can calculate "*n*" and hence the OPBM in terms of base shear would be evaluated using Eq. (27).

$$OPBM = \alpha\, EV \qquad (27)$$

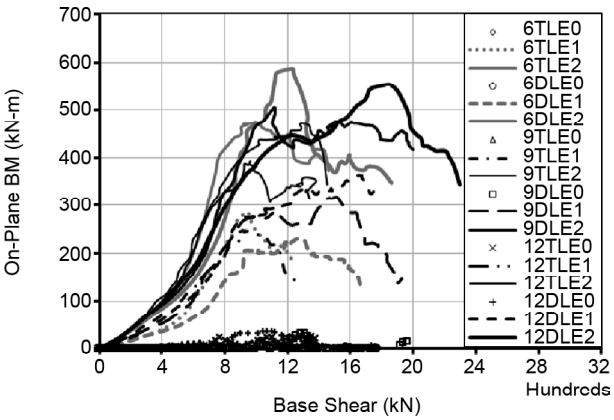

a) Distribution of OPBM Versus Base Shear

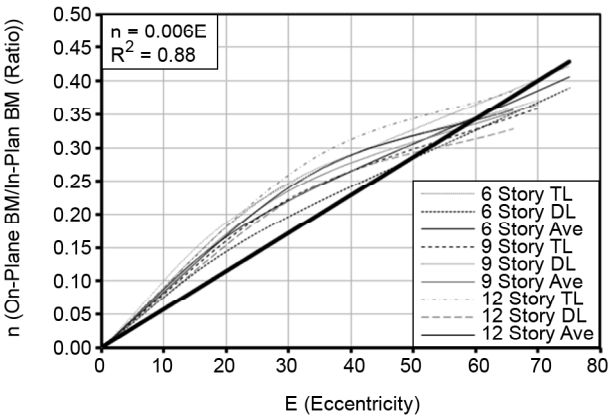

b) Ration of OPBM/IPBM Versus Eccentricity

Figure 9. Effect of eccentricity on the on-plane bending moment exerted to shear wall.

4.2. Nonlinear Time History Analysis

For seismic input, the horizontal components of ground accelerations records of three well-known Iran earthquakes, Bam (2004), Tabas (1987) and Kojour (2004) have been used. These earthquakes cover acceptable range of frequency content and duration. For the purpose of comparing between frequency content of records and in order to eliminate the differences among the peak ground accelerations, all the records have been scaled according to the Iranian standard 2800 [21]. For all records, the normalized elastic response spectra and the average values considering the viscous damping coefficient equal to 5% are depicted in Figure (10). In order to evaluate the effect of shear wall's eccentricity on seismic performance of studied frames, top displacement, base shear, and on-plane shear were calculated for each earthquake. It is required to note that the history of all structural responses cannot easily be shown in one set of coordinate system. Therefore, it was decided to prepare the envelop curves for history responses

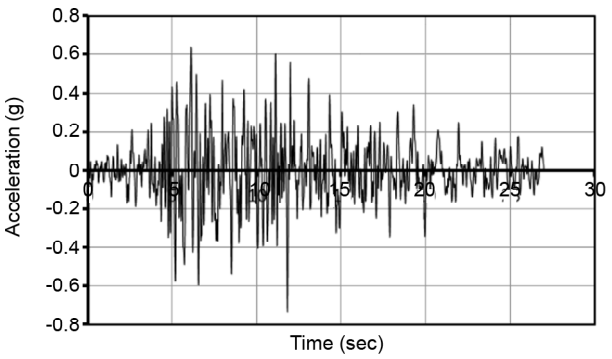

a) Bam Acceleration

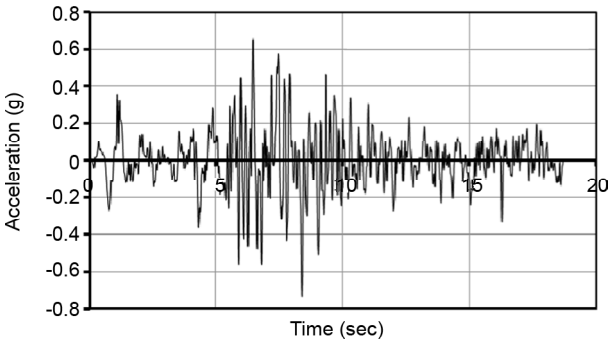

b) Tabas Acceleration

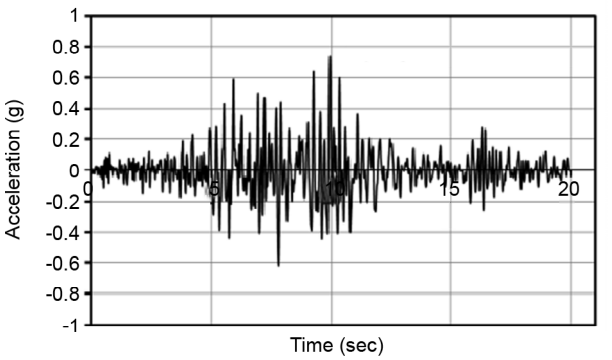

c) Kojour Acceleration

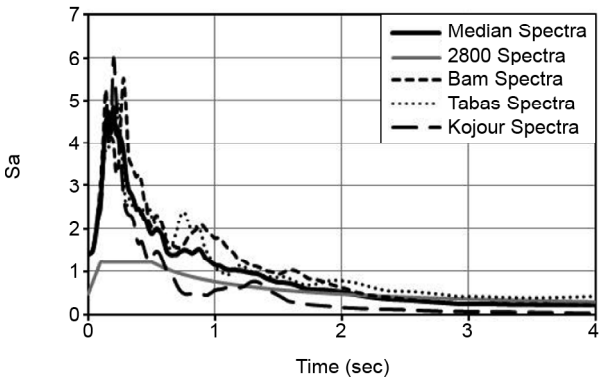

Figure 10. Scaled time history acceleration and 5% damping spectrum for the used earthquakes.

shown in Figure (11).

For comparison maximum values of top displacement, base shear and on-plane shear for all structures are drawn and presented in Figures (12) to (14).

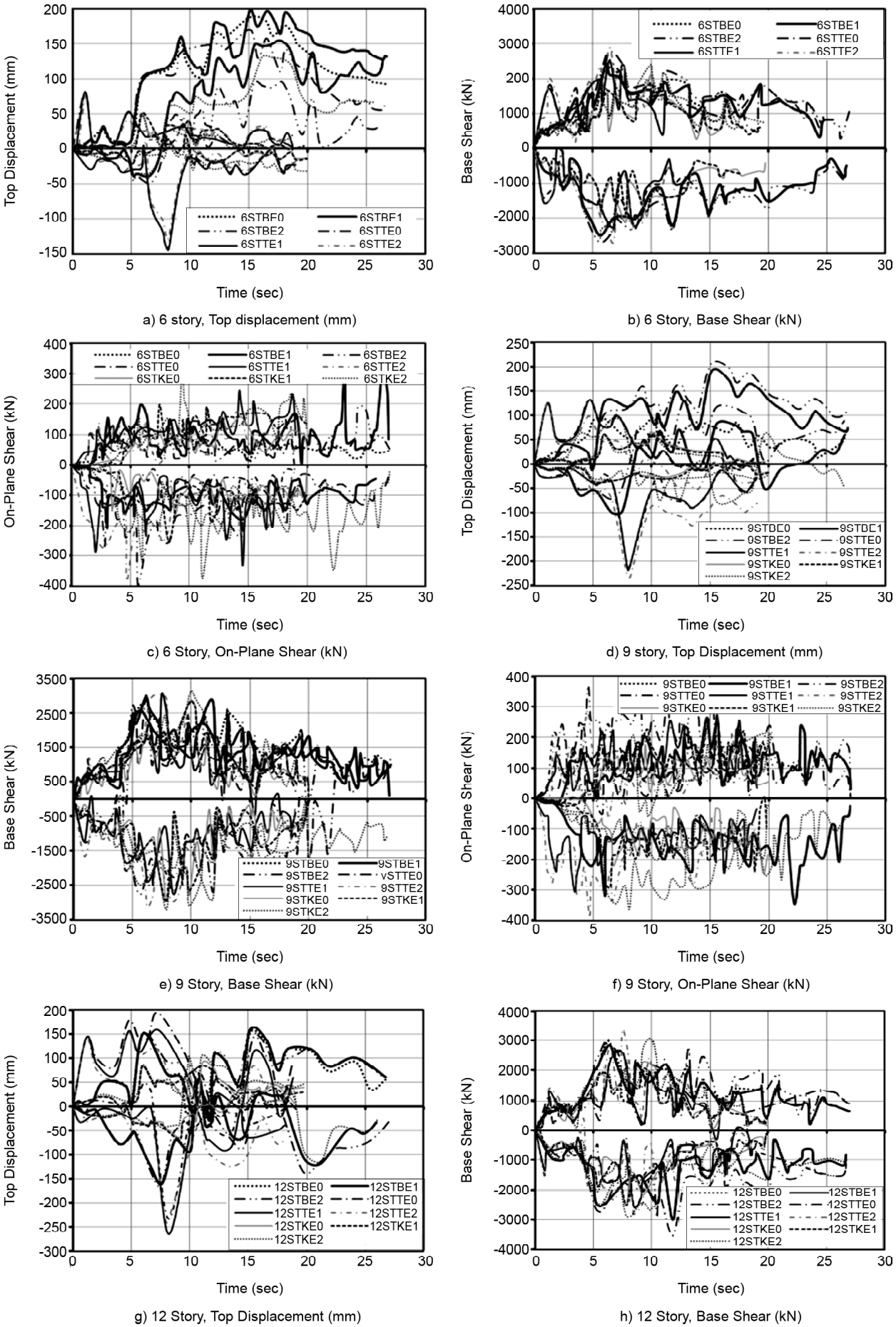

Figure 11. Envelop curves of nonlinear time history responses, all structures.

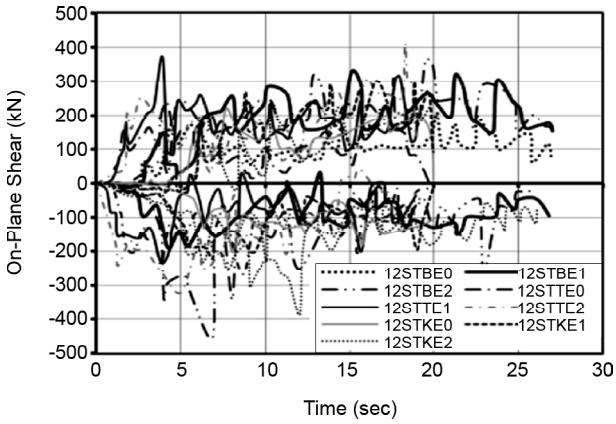

i) 12 Story, On-Plane Shear (kN)

Figure 11. Continue.

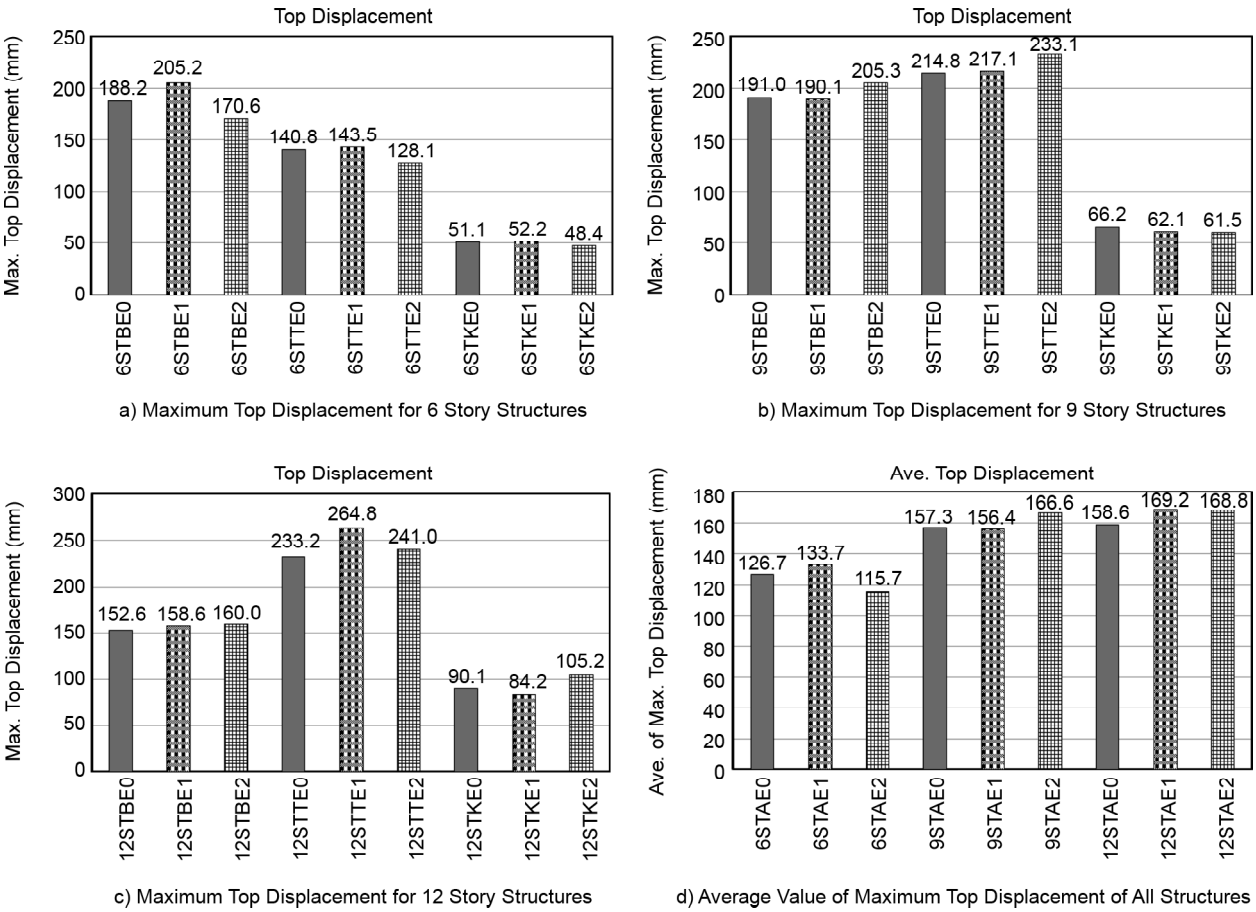

Figure 12. Maximum top displacement from nonlinear time history analysis.

Figures (12a), (12b) and (12c) illustrate the variation of maximum top displacement with respect to the earthquake records. Although this variation is somehow sensitive to each record, it is clear that for each record there is no significant effect of eccentricity for all categories of structures. In addition, it is shown that the displacement slightly increases as the height of the structure increases. On the other hand, the shear wall's eccentricity has no significant effect on the average value of maximum top displacement, Figure (12d).

Figure (13) shows the low effect of eccentricity on base shear. Eccentricity of shear wall has no significant effect on maximum base shear of 6 story structures. In the case of 9 story structures, the base shear increases as the eccentricity increases. This is

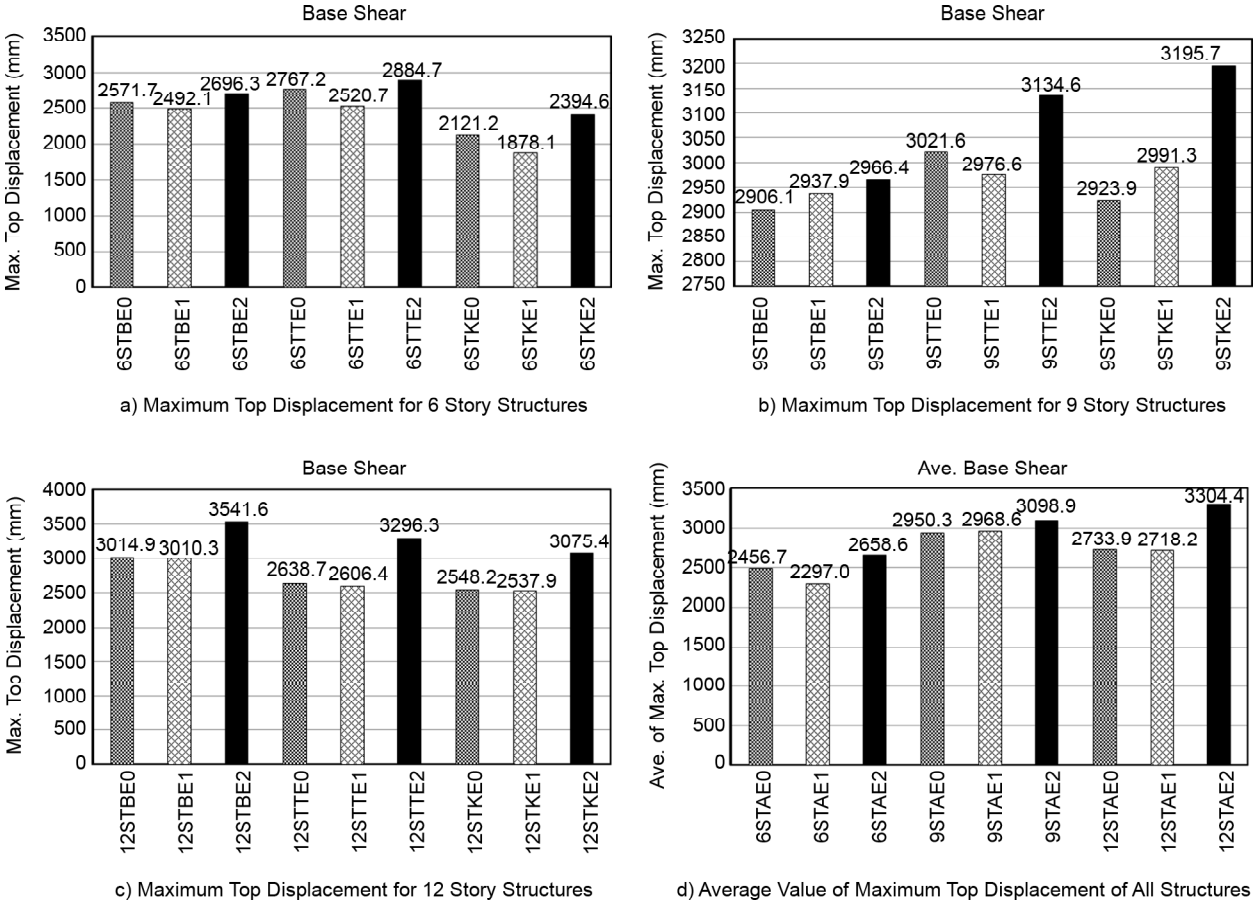

Figure 13. Maximum base shear from nonlinear time history analysis.

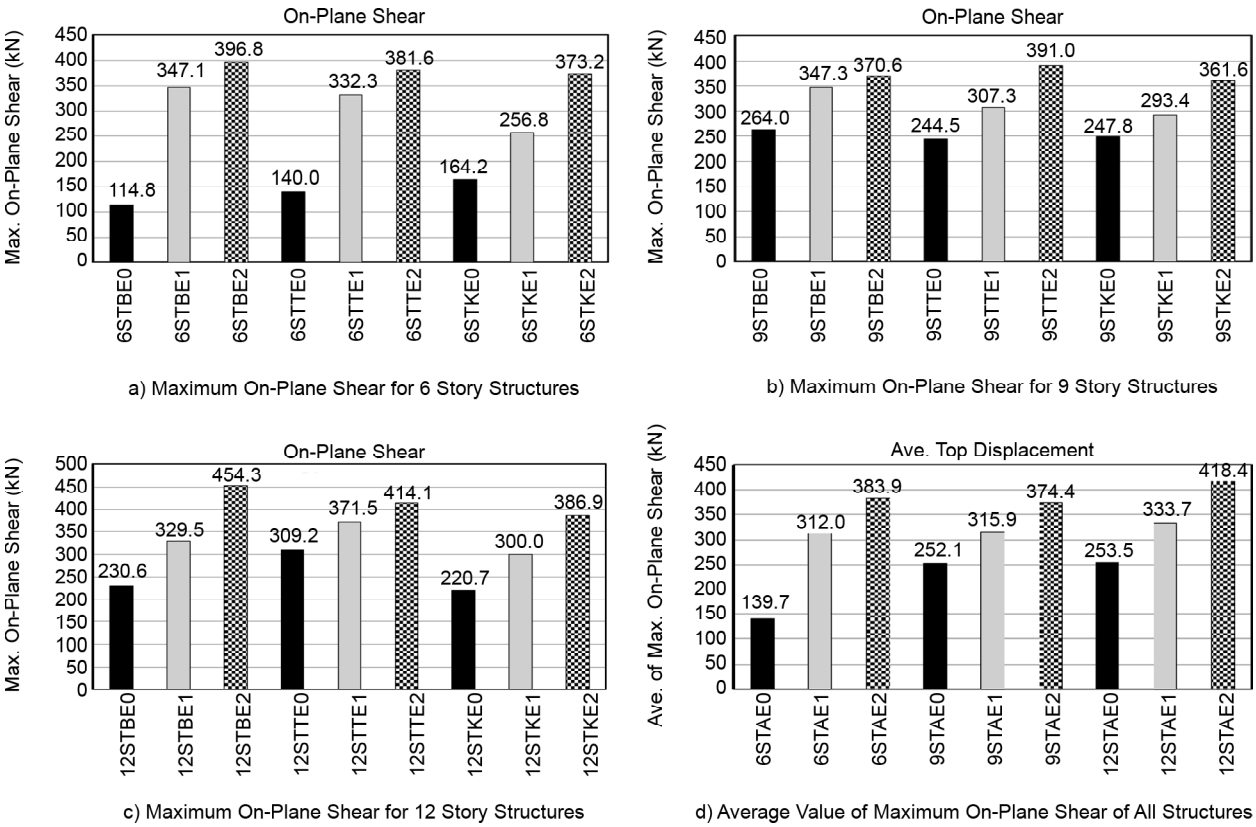

Figure 14. Maximum base shear from nonlinear time history analysis.

slightly the same for 12 story structures. The history of base shear in all 12 story structures indicates that maximum base shear in all earthquakes are approximately equal. The comparison between the average values of base shear indicates that the base shear increases as the eccentricity and the height of structure increase. Contrary to top displacement and base shear, the results of nonlinear time history analyses indicate that eccentricity of shear wall has significant effect on on-plane shear. According to Figure (14), the on-plane shears of 6 story structures increase significantly with the eccentricity, which is the same for 9 and 12 story structures as well. The average values of on-plane shear show in Figure (14d) clearly indicate the considerable increase of on-plane shear due to the increase of eccentricity and height of structure.

5. Conclusion

In this study, the effect of shear wall's eccentricity on seismic performance of RC dual system is studied. The nonlinear static and time history analyses were carried out for 6, 9 and 12 story structures with three various amount of shear wall's eccentricity. Based on this study, presented in this article, the following conclusions are drawn:

- Numerical modelling estimates well the capacity curve for tested shear walls.
- From capacity curves it is evident that the eccentricity of shear wall has no significant effect on elastic state of behaviour and the nonlinear behaviour is under the influence of structural height.
- All structures have more response to the distributed lateral load rather than inverted triangle lateral load and this is more pronounced by increasing the height of the structure.
- By increasing the amounts of eccentricity and story height, the ratio of torsional moment exerted to the boundary element of shear wall increases.
- The results of nonlinear time history analyses indicate that eccentricity of shear wall has no significant effect on top displacement and base shear of frame, but it is the cause of producing on-plane shear in shear wall.
- The out-of-plane displacement due to the torsion created by the eccentricity of the wall did not appear to affect the response of the structure.

References

1. Orakcal, K., Massone, L.M., and Wallace, J.W. (2006). Analytical Modeling of Reinforced Concrete Walls for Predicting Flexural and Coupled-Shear-Flexural Response, University of California. PEER Report.
2. Paulay, Th. and Priestley, M.J.N. (1992). Seismic Design of Reinforced Concrete and Masonry Building, John Wiley & Sons Inc., New York.
3. Abrams, D.P. (1980). Experimental Study of Reinforced Concrete Frame-Wall Structure Subjected to Strong Earthquake Motions, *Proceedings of 7th World Conference on Earthquake Engineering*, 191-198.
4. Naeim, F. (2002). The Seismic Design Handbook, 2nd Edition, Springer.
5. Liao, Wen-I. et al. (2004). Experimental Studies of High Seismic Performance Shear Wall, *Proc. of 13th World Conf. on Earthquake Engineering*, Vancouver, B.C Canada, Paper No. 501.
6. Maheshw, A. and Santhakumar, A.R. (2004). Capacity Design for Tall Building with Mixed System, *13th World Conf. on Earthquake Engineering*, Vancouver, B.C Canada, Paper No. 2367.
7. Ranai, R.J.L. and Zekioglu, A. (2004). Pushover Analysis of 19 Story Concrete Shear Wall Building, *13th World Conf. on Earthquake Engineering*, Vancouver, B.C Canada, Paper No. 133.
8. ACI Committee 318 (2002). Building Code Requirements for Structural Concrete (ACI318-02), American Concrete Institute, Farmington, Mich.
9. Issue No. 120 (2002). Iranian Concrete Code (ABA), Iranian Management Organization, 6th Edition, Tehran, Iran.
10. Larry Roland Jimenez (1989). Strengthening of Reinforced Concrete Frame Using an Eccentric Wall, MSc, thesis, University of Texas at Austin.
11. Bahari, A. (2009). Nonlinear Behaviour of Eccentric Coupled Beams with Coupled Shear Wall, MSc Thesis, TarbiatModares University, Tehran, Iran.

12. Habbit, Karlsson & Sorensen (2009). Abaqus Theory Manual Version 6.9.1.

13. Lee, J. and Fenves, G.L. (1998). Plastic-Damage Model for Cyclic Loading of Concrete Structures, *ASCE, Journal of Engineering Mechanics*, **124**, 892-900.

14. Mander, J.B., Priestley, M.J.N., and Park, R. (1989). Theoretical Stress-Strain Model for Confined Concrete, *Journal of Structural Engineering*, **114**(8), 1804-26.

15. Martinez-Rueda, J.E. and Elnashai, A.S. (1997). Confined Concrete Model under Cyclic Load, *Materials and Structures*, **30**, 139-47.

16. Menegotto, M. and Pinto, P.E. (1973). Method of Analysis for Cyclically Loaded R.C. Plane Frames Including Changes in Geometry and Non-Elastic behavior of Elements under Combined Normal Force and Bending, Symposium on the Resistance and Ultimate Deformability of Structures Acted on by Well Defined Repeated Loads, Zurich, Switzerland; International Association for Bridge and Structural Engineering, 15-22.

17. Filippou, F.C., Popov, E.P., and Bertero, V.V. (1983). Modeling of R/C Joints under Cyclic Excitations, *Journal of Structural Engineering*, **109**(11), 2666-84.

18. Fragiadakis, M. (2001). Nonlinear Material Modeling of Reinforcement Steel Bars under Transient Loading, MSc Dissertation, Department to Civil and Environmental Engineering, Imperial College, London, UK.

19. Oesterle, R.G., Fiorato, A.E., Johal, L.S., Carptenter, J.E., Russell, H.G., and Corley, W.G. (1976). Earthquake-Resistant Structural Walls-Tests of Isolated Walls, Report to National Science Foundation, Construction Technology Laboratories, Portland Cement Association, Skokie, Ill, 315p.

20. Thomsen, J.H. and Wallace, J.W. (1995). Displacement-Based Design of Reinforced Concrete Structural Walls: An Experimental Investigation of Walls with Rectangular and T-Shaped Cross-Sections, Report No. CU/CEE-95/06, Department of Civil Engineering, Clarkson University, Postdam, New York.

21. BHRC Standard 2800 (2005). Iranian Code of Practice for Seismic Resistant Design of Building, Building and Housing Research Centre, 3rd Edition, Tehran, Iran.

22. FEMA 356 (2000). Prestandard and Commentary for the Seismic Rehabilitation of Building, American Society of Civil Engineering, Reston, VA.

Notations

A_s : Total Area of steel bars for column section
b_b : Beam width
b_c : Column width
b_f : Flange width
d_b : Beam depth
d_c : Column depth
d_f : Flange depth
c : Coefficient of cohesion
C : Damping matrix
e : Eccentricity parameter (defines the rate at which the function approaches the asymptote)
E : Elastic modulus (a rank four tensor)
E_o : Initial (undamaged) elastic modulus (a rank four tensor)
F : Isotopic function in the stress space / first-degree homogeneous function
f_c : Uniaxial characteristic compressive strength of concrete
f'_{ct} : Uniaxial characteristic tensile strength of concrete
f_y : Uniaxial yield strength of steel bars
G : Flow potential
k : Scalar stiffness degradation variable
K : Stiffness matrix
K^{el} : Degraded or damaged elastic stiffness
K_o^{el} : Initial or undamaged elastic stiffness
k_c : Damage parameter in compression
k_t : Damage parameter in tension
l_e : The smallest element dimension
L_w : Web length
m : Ratio of torsional moment to base shear
M : Mass matrix
n : ratio of on-plane bending moment to base shear
p : Normal stresses at interface (contact pressure)
$\bar{p}$: Effective hydrostatic pressure
$\bar{q}$: Von Missies equivalent effective stress
R : Load vector in time domain

$\bar{s}$: Deviatoric part of the effective stress tensor
T: Fundamental period
t_w: Flange thickness
X: Displacement in time domain
$\dot{X}$: Velocity in time domain
$\ddot{X}$: Acceleration in time domain
α: Material parameters, determine the shape of the hill yield surface
β: Material parameters, determine the shape of the hill yield surface
γ: Material parameters, determine the shape of the hill yield surface
Δt: Time increment
Δt_{cr}: Critical time increment
ε: Strain tensor
ε^{el}: Elastic part of strain tensor
ε^{pl}: Plastic part of strain tensor
$\dot{\varepsilon}$: Total strain rate
$\dot{\varepsilon}^{el}$: Elastic part of strain rate
$\dot{\varepsilon}^{pl}$: Plastic part of strain rate
$\tilde{\varepsilon}_c^{pl}$: Equivalent plastic strains in compression (Hardening variable)
$\dot{\tilde{\varepsilon}}_c^{pl}$: Equivalent plastic strain rate in compression
$\tilde{\varepsilon}_t^{pl}$: Equivalent plastic strains in tension (Hardening variable)
$\dot{\tilde{\varepsilon}}_t^{pl}$: Equivalent plastic strain rate in tension
η: Material parameters, determine the shape of the hill yield surface
$\dot{\lambda}$: Non-negative plastic multiplier
μ: Coefficient of friction defined as a function of the contact pressure
v_b: Brick poisson ratio
v_m: Mortar poisson ratio
ρ: Density of material
ρ_c: Reinforcement percentage in compression
ρ_t: Reinforcement percentage in tension
σ: Stress tensor
$\bar{\sigma}$: Effective stress
σ_{bo}: Uniaxial compressive stress at failure
σ_c: Uniaxial compressive strength of concrete
$\bar{\sigma}_c$: Effective compressive stress
σ_t: Uniaxial tensile strength of concrete
$\bar{\sigma}_t$: Effective tensile stress
σ_y: Von Misses yield stress of the material
σ_{to}: Uniaxial tensile stress at failure
$\hat{\bar{\sigma}}_{\max}$: Algebraically maximum eigenvalue of $\bar{\sigma}$
τ: Tangential stresses exist at the interface
τ_{crit}: The critical shear stress
$\tau_{\max}$: The maximum shear stress
ϕ: Angle of friction
ψ: Dilatation angle